

Photodetachment of K^-

Chien-Nan Liu*

Max Planck Institute for the Physics of Complex Systems, Nöthnitzer Strasse 38, D-01187 Dresden, Germany

(Received 26 February 2001; revised manuscript received 11 June 2001; published 12 October 2001)

Eigenchannel R -matrix calculation results are presented for the photodetachment of K^- in the energy region between the $K(5s)$ and $K(7p)$ thresholds. Present results are compared with prior experimental studies, including the recent relative $K(5s)$ partial cross section measurements of Kiyani *et al.* [Phys. Rev. A **84**, 5979 (2000)], and resonances observed in electron-potassium scattering. Detailed analyses and identifications of $^1P^o$ resonance structures are presented. Comparisons with H^- and other alkali-metal negative ions provide further information on the structure and dynamics of negative ions.

DOI: 10.1103/PhysRevA.64.052715

PACS number(s): 32.80.Gc, 31.25.Jf

I. INTRODUCTION

Photodetachment plus excitation of atomic negative ions is a fruitful means of observing correlated doubly excited states. H^- has been most intensively studied theoretically and experimentally due to its importance of a fundamental three-body system [1]. Because their structures of valence electrons resemble the one of H^- , metastable He^- [2,3] and light alkali-metal negative ions, such as Li^- [4,5] and Na^- [6,7], have also been a focus of a number of recent theoretical and experimental studies. (Note that only the most recent references are given; readers may consult these references for earlier works.) The spectrum of doubly excited states in K^- is relatively unexplored. Most of the previous theoretical and experimental studies on photodetachment of K^- [8] and electron-potassium scattering [9] are limited to the energy region from threshold to the vicinity of the $K(4p)$ threshold, the first excited state of neutral potassium. Since the spin-orbit splitting of the $K(4p)$ doublet is about 7 meV, the fine structure is resolved in experimental measurements and requires theoretical calculations in jj coupling to give accurate descriptions. Very recently, Kiyani *et al.* reported experimental measurements for the processes $K^- + \gamma \rightarrow K(5s) + e^-$ for the energy region from above the $K(6p)$ threshold to the vicinity of $K(5f)$ threshold, revealing seven resonances [10]. More interestingly, they found an anomalous behavior that the widths of the four resonances observed below the $K(5f)$ threshold do not decrease monotonically, as predicted by a semiclassical model describing that the doubly excited states of nonhydrogenic negative ions are formed as bound states of an induced dipole potential [2,11].

In this paper, eigenchannel R -matrix calculations for photodetachment of K^- using a two-active-electron model are presented. The study covers the energy region from the vicinity of the $K(5p)$ threshold to just above the $K(7p)$ threshold. Since the spin-orbit splitting of these high-lying excited states of neutral potassium are small, LS coupling is sufficient. Results for total and partial cross sections and for the photoelectron angular distribution asymmetry parameter

β are presented. For energies in the vicinity of the $K(5d)$ and $K(5f)$ thresholds, present results are compared with recent experimental measurements of Kiyani *et al.* [10]. The main focus of this paper is on the identification and analysis of the resonance structures that appear in the energy region studied, shedding light on resonance formation in negative ions. We will address the differences of structures between H^- , a pure three-body system with distinct approximate symmetry [12–14], and the alkali-metal negative ions, which can be accurately described by a two-active-electron model.

II. THEORY

The eigenchannel R -matrix method [15,16] and a two-active-electron model are employed in this study. For the energy region below the double detachment threshold, alkali-metal negative ions may be adequately treated as two active electrons moving in a central field resulting from the nuclear charge and the frozen inner shell electrons. This method has proved successful in previous applications to H^- , metastable He^- and alkali-metal negative ion photodetachment [3,5,6,17,18]. The method has been described in detail in Ref. [18] and the method for analyzing doubly excited-state resonances and their effects has been described in Ref. [3]. Thus, we present here only a brief overview of the eigenchannel R -matrix method and of the methods for analyzing excited, two-electron resonances.

A. Brief overview of the eigenchannel R -matrix method

The eigenchannel R -matrix method [15,16] aims to determine variationally an orthogonal and complete basis set of wave functions, the *eigenchannel wave functions*, at given energy E , whose normal logarithmic derivatives are constant across a reaction surface S enclosing a reaction volume V . For treatments of two-electron excitations, the reaction volume V is that part of six-dimensional configuration space for which both electrons lie within a sphere of radius r_0 . In practice, for each range of excitation energy, r_0 is chosen to be sufficiently large that the probability of both electrons being outside r_0 is negligible. Thus, r_0 has to be large enough to encompass all possible doubly excited-state wave functions in the energy range considered. The complicated many-electron interactions within V are treated by

*Current address: Department of Physics, Cardwell Hall, Kansas State University, Manhattan, Kansas 66506.

TABLE I. Empirical parameters for the K^+ model potential.^a

l	a_1	a_2	a_3	r_c (a.u.)
0	5.398 774	15.041 973	2.129 288	0.8
1	4.174 006	6.691 497	1.767 564	0.8
2	6.163 766	7.605 658	2.027 534	0.8
≥ 3	10.016 154	0.783 871	1.562 949	0.8

^aCf. Eq. (1).

bound state, configuration interaction (CI) techniques using a basis of independent electron orbital wave functions obtained from a model potential for the K^+ core and LS coupling to represent the many-electron wave function. The model potential has the form,

$$V(r) = -\frac{1}{r}[Z_c + (Z - Z_c)e^{-a_1 r} + a_2 r e^{-a_3 r}] - \frac{\alpha_c}{2r^4}(1 - e^{-(r/r_c)^3})^2. \quad (1)$$

For the K^- calculation, the nuclear charge is $Z=19$, the charge of the K^+ core is $Z_c=1$, and the polarizability of the K^+ core is given by the value, 5.457 a.u. [19]. The empirical parameters (a_1, a_2, a_3, r_c) depend on electron orbital angular momentum l and are fitted using a least-squares method to reproduce the experimentally measured energy levels of the K atom [20]. The values used in the present calculation are given in Table I. The calculated energy levels using the model potential are presented and compared with experimentally observed results [20] in Table II, indicating the accuracy of these energies and the wave functions as well.

At a given energy E , one describes the wave function inside the reaction volume as a linear combination of the *eigenchannel wave functions* thus generated. Outside r_0 , it is

TABLE II. Energy levels of $K(nl)$. Energies are shown with respect to the K^+ threshold in a.u. The experimental energies are weighted average of all fine-structure levels.

nl	Calc. Energy	Expt. Energy ^a
4s	-0.1595161	-0.1595164
4p	-0.1001545	-0.1001545
5s	-0.06371234	-0.06371242
3d	-0.06139328	-0.06139328
5p	-0.04690452	-0.04690459
4d	-0.03468437	-0.03468437
6s	-0.03444187	-0.03444182
4f	-0.03135650	-0.03135653
6p	-0.02735725	-0.02735720
5d	-0.02198149	-0.02198150
7s	-0.02157669	-0.02157684
5f	-0.02006194	-0.02006193
5g	-0.02001394	-0.02001371
7p	-0.01793623	-0.01793618

^aReference [20].

assumed there is only a single electron, and thus, only single-detachment processes are considered. All long-range multipole interactions in the outer region are treated numerically by close-coupling procedures in order to obtain a basis set of multichannel wave functions that describe the outgoing electron and the residual atom [18]. By thus treating the long-range multipole interactions, the effects due to the polarization of the residual atom are included. By matching linear combinations of the multichannel basis functions for the inner and outer regions at the reaction surface, one may determine the exact final-state wave function that satisfies the incoming wave boundary condition. Further details of the method are presented in Ref. [18].

B. Identification of resonances and the corresponding doubly excited states

In order to obtain predictions for resonance energies and widths for comparison with other theoretical and experimental results, two different approaches are used. For a single isolated resonance, one may perform a least-squares fitting of the calculated partial cross section to a resonance profile formula [21–23]. However, in the energy region where a resonance is not completely separated from adjacent features due to thresholds or other resonances, one may analyze instead the eigenphase sum as a function of energy [24,25]. Note, that in some instances in which resonances are located close to a threshold, the overlap of changes in the eigenphase sum with the threshold prevents us from predicting a width.

To characterize the states responsible for the resonances in the cross-section spectra, a standard projection operator method is used. Doubly excited states associated with the nl threshold are obtained by diagonalizing the Hamiltonian using a basis that excludes all one-electron orbitals corresponding to open channels. Those discrete states that lie below the nl threshold are the doubly excited states that manifest themselves as resonances in the cross sections. The doubly excited state wave functions are checked by a projection procedure in which cross sections are calculated using a final-state wave function that is orthogonalized to these doubly excited states. By examining its effects on the cross section, one can make sure that removed doubly excited state is indeed responsible for a specific resonance.

C. Numerical details

The radius of the R -matrix sphere, r_0 is chosen to be 180 a.u.. This radius is large enough to encompass the doubly excited states in the considered energy range. Inside the R -matrix sphere, 58 closed-type (i.e., zero at the radius r_0) and two open-type (i.e., nonzero at the radius r_0) one-electron orbital wave functions are calculated for each of the orbital angular momenta l , where $0 \leq l \leq 6$. In total, 2504 closed-type, two-electron configurations are included in the calculation for the final-state wave function. For each channel in which one electron may escape from the reaction volume, two open-type orbitals for the outer electron are included in addition to the closed-type basis set. For a given photon energy, besides all open channels, closed channels having the inner electron at the next higher-principal quan-

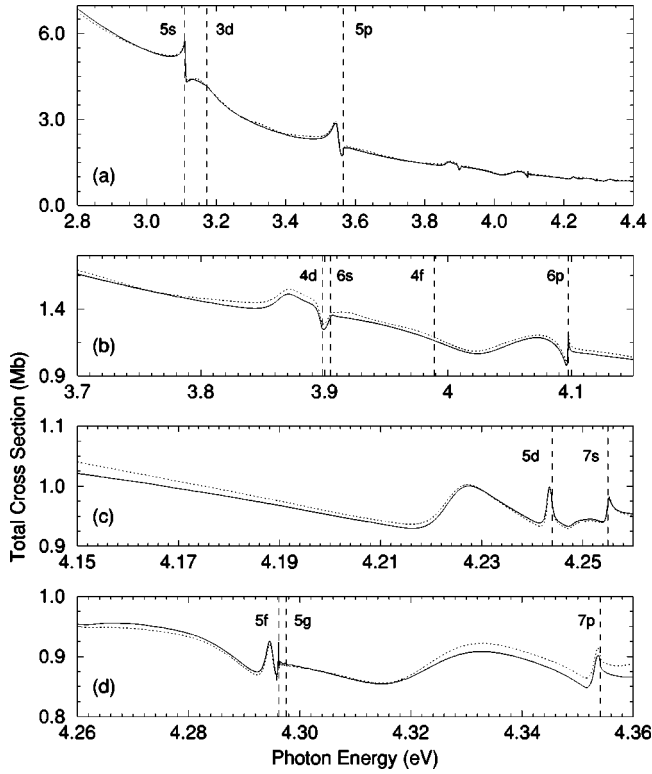


FIG. 1. (a) Total cross section for photodetachment of K^- . Present dipole velocity (length) results are plotted using the solid (dotted) line. (b)–(d) Total cross section in the energy regions near excited-state thresholds, $K(nl)$, whose positions are indicated by vertical dashed lines.

tum number state are also included in the calculation. Finally, the value for the electron affinity for K^- employed in this paper is 501.459 meV [26].

III. RESULTS

Figure 1(a) shows an overview of the present results for the total cross section for photodetachment of K^- in the photon energy range from 2.8 to 4.4 eV. This energy range encompasses the region from below the $K(5s)$ threshold to the $K(7p)$ threshold. As one may see, the total cross section diminishes rapidly as the photon energy increases, and so do the resonance features. Figure 1(b)–(d) examine regions where weaker but richer resonance structures near higher-excited thresholds of K are found in the present calculations. Detailed analyses for each of the energy regions corresponding to each panel in Fig. 1 are presented in the following sections. A complete list of all $^1P^o$ resonances that present calculations predict in this energy region are presented in Table III with their energy positions and widths.

A. K^- photodetachment near the $K(5s)$, $3d$, and $5p$ thresholds

The most prominent features in the total cross section in the energy region shown in Fig. 1(a) are the two resonances in the vicinity of the $K(5s)$ and $K(5p)$ thresholds, located at 3.11019 and 3.55076 eV, respectively. The former is located at just 1.77 meV above the $K(5s)$ threshold, and is thus

TABLE III. $^1P^o$ resonance energies and widths of K^- in the energy region below the $K(7p)$ threshold.

Present Results			Experiment ^a		
$\hbar\omega$ (eV)	E_{4s} (eV) ^b	Γ (meV)	Label	$\hbar\omega$ (eV)	Γ (meV)
3.11019	2.60872	4.4687			
3.55076	3.04929	19.0179			
3.86853	3.36706	24.1621			
3.89414	3.39267	4.3301			
4.03092 ^c	3.52946	80.0404 ^c			
4.09714	3.59567	1.0800			
4.20712	3.70565	11.6913			
4.22383	3.72236	12.7825	<i>a</i>	4.2229(4)	14.5(6)
4.24330	3.74183	1.4376	<i>b</i>	4.24329(6)	1.41(8)
4.24750 ^d	3.74603	3.1870	<i>c</i>	4.2486(4)	3.5(7)
4.25498	3.75351	1.2817			
4.27590 ^e	3.77443		<i>d</i>	4.292(2)	10(2)
4.29472	3.79325	1.4722	<i>e</i>	4.2945(1)	1.5(2)
4.2958031	3.79433	0.002	<i>f</i>	4.29576(4)	0.10(8)
4.29606	3.79459	0.1420	<i>g</i>	4.2960(2)	0.30(3)
4.32339 ^c	3.82192	27.7183 ^c			
4.35350	3.85203				

^aReference [10].

^bEnergy with respect to the $K(4s)$ ground state.

^cResulting from fitting the calculated total cross section to a resonance profile formula [cf. Eq. (2)].

^dShape resonance.

^eDoubly excited-state energy obtained by the standard projection operator method.

characterized as a shape resonance. It is produced by a doubly excited state with dominant $5snp$ configurations, including $5s7p$ (26.8%), $5s8p$ (24.9%), and $5s9p$ (17.9%). The one close to the $K(5p)$ threshold is produced by a doubly excited state whose leading configuration components are $5p6s$ (32.3%), $5p7s$ (32.0%), and $5p4d$ (10.6%). These two doubly excited states are obtained by applying the standard projection operator method with respect to the $K(5s)$ and $K(5p)$ thresholds, respectively.

In the vicinity of the $K(5s)$ threshold, Johnston and Burrow observe a resonance at 2.60 eV above the $K(4s)$ ground state, equivalent to a photon energy of 3.10 eV in the photodetachment spectra of K^- , with a width of 60 meV [27]. They suggested a term designation of $5s3d\ ^3D$ due to its proximity to the resonance observed in electron-potassium scattering measurements by Eyb, who observed an angular distribution characteristic of a d -wave [28]. While the measured width for the 3D resonance is about 60 meV, the predicted $^1P^o$ resonance at 3.11019 eV is probably either too weak to have been observed by them, or obscured by the 3D resonance, in electron-potassium scattering experiments. Note that there are only three resonances observed so far in electron-potassium scattering in the neighborhood of the $K(5s)$ and $K(3d)$ thresholds. The other two were also ob-

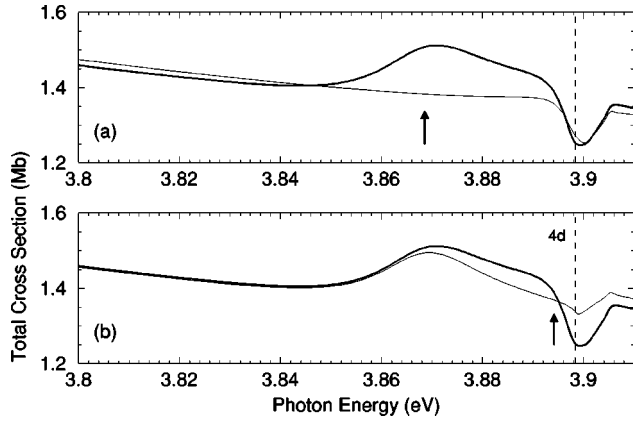


FIG. 2. Total cross section near the K($4d$) threshold. Thick curve: present results in dipole velocity approximation. Thin curve: results obtained by removing one doubly excited state from the calculation. The vertical dashed lines indicate the locations of the thresholds. (a) The doubly excited state responsible for the resonance at 3.868 53 eV removed. (b) The doubly excited state responsible for the resonance at 3.894 14 eV removed. The arrows indicate the energy locations of the doubly excited state that has been removed from the cross section result shown in the thin curve.

served by Eyb at 2.4 and 2.68 eV above the K($4s$) state, or equivalently 2.9 and 3.18 eV photon energies in the photodetachment spectra of K^- , and were assigned as S and P or F states, respectively [28].

The total cross section shows a characteristic threshold behavior corresponding to detachment into an s -wave continuum at the K($5p$) threshold. According to Wigner's threshold law [29], the photodetachment cross section σ should behave near a threshold as

$$\sigma \propto k^{2l+1}, \quad (2)$$

where k and l are, respectively, the linear and angular momenta of the outgoing electron. Detachment into an s -wave continuum exhibits a sharp onset in the cross section because of the threshold behavior $\sigma \propto (E - E_{\text{threshold}})^{1/2}$. Such characteristic threshold behavior allows experimentalists to measure electron affinities with very high precision. In the present case, the total cross section near the K($5p$) threshold takes the form of a upward step.

B. K^- photodetachment near the K $4d$, $6s$, $4f$, and $6p$ thresholds

As shown in Fig. 1(b), the total cross section exhibits a feature apparently resulting from two overlapping resonances in the energy region just below the K($4d$) threshold. Indeed, the eigenphase sum analysis reveals two resonances at 3.868 53 and 3.894 14 eV, respectively. In order to account for these resonances, the standard projection operator method was used to search for doubly excited states below the K($4d$) threshold. As a result, two doubly excited states are found in this energy region. The effects of each of these two states on the total cross section are illustrated in Fig. 2. While the state lower in energy is responsible for the more prominent peak, the other one produces the shoulderlike fea-

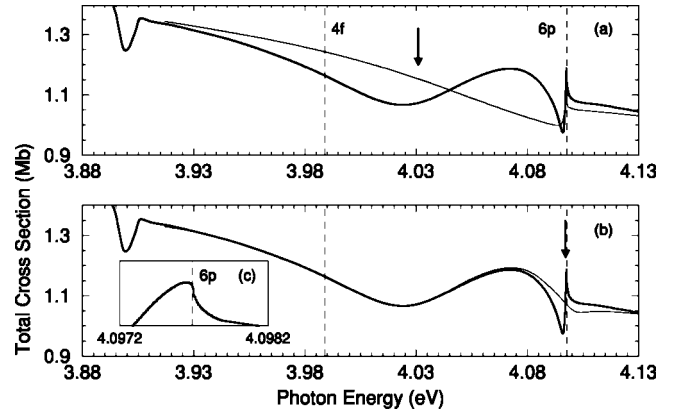


FIG. 3. Total cross section near the K($4f$) threshold. Thick curve: present results in dipole velocity approximation. Thin curve: results obtained by removing one doubly excited state from calculations. The vertical dashed lines indicate the locations of the thresholds. (a) The doubly excited state responsible for the resonance at 4.030 92 eV removed. (b) The doubly excited state responsible for the resonance at 4.097 14 eV removed. (c) Present results in an energy region within ± 0.5 meV of the K($6p$) threshold. The arrows indicate the energy locations of the doubly excited state that has been removed from the cross-section result shown in the thin curve.

ture. The overlapping of the two resonances implies weak interaction between the two responsible states. Indeed, although both states have strong configuration mixing, their configuration components indicate different characters. While the resonance located at 3.868 53 eV results from a doubly excited state with the leading configurations of $4d6p$ (31.1%) and $4d7p$ (16.5%), the other located at 3.893 44 eV is dominated a state having strong $6s7p$ (32.1%) and $6s8p$ (18.8%) components.

While there is no visible threshold behavior associated with the K($4f$) threshold at 3.988 87 eV, no resonance is associated with the threshold. It is worthwhile to note, the K($4f$) excited state has a negative polarizability, implying a repulsive asymptotic behavior the induced dipole potential of this state. Therefore, it is less likely to support a resonance series. However, a negative polarizability does not forbid the formation of doubly excited resonances since the interaction in the region close to the nucleus could be attractive due to electron-electron correlation. For example, it has been found in the case of Na that a resonance is associated with the Na($5p$) excited state having a negative polarizability [6].

The resonance structure in the total cross section in the energy region below the K($6p$) threshold is better illustrated in Fig. 3. In the vicinity of the K($4f$) threshold, the total cross section is actually dominated by a broad window resonance, while another much narrower resonance appears just below the K($6p$) threshold. Applying the standard projection operator method with respect to the K($6p$) threshold reveals two doubly excited states. Effects of each of these two resonances on the total cross section are also shown in Fig. 3, indicating that both resonances are produced by doubly excited states associated with the K($6p$) state. The resonance located at 4.030 92 eV has a very broad width, which extends

TABLE IV. Dipole polarizabilities of $K(nl)$.

nl	Dipole polarizability (a.u.)
4s	307
4p	619
5s	4996
3d	1401
5p	7204
4d	35665
6s	32866
4f	-11585
6p	44170
5d	193034
7s	139013
5f	3936137
5g	-3097696
7p	180730

over the $K(4f)$ threshold [cf. Fig. 3(a)]. While the state responsible for this resonance is dominated by the configurations $6p7s$ (30.2%), $6p5d$ (21.3%), and $6p8s$ (15.4%), the other resonance located at 4.09656 eV [cf. Fig. 3(b)] is produced by a doubly excited state dominated by the configurations $6p9s$ (30.4%), $6p8s$ (19.4%), and $6p10s$ (14.7%). Their similar $6pns$ configuration compositions indicate that both states belong to the same series that converges to the $K(6p)$ threshold.

Figure 3(c) shows the region close to the $K(6p)$ threshold, illustrating a characteristic threshold behavior corresponding to detachment into an s -wave continuum. In the present case, the total cross section near the $K(6p)$ threshold takes the form of a downward step, instead of a cusp. The validity of the threshold law is restricted to an extremely narrow energy range of 0.1 meV, so it is difficult to observe the feature experimentally. It has been pointed out that the huge dipole polarizabilities of excited atomic states (cf. Table IV) result in the small range of validity of the Wigner law [18]. The experimental report [10] of a cusp structure at the $K(6p)$ threshold is most likely due to the narrow resonance.

C. K^- photodetachment near the $K(5d)$ and $7s$ thresholds

Partial cross sections for all open channels in the energy region below the $K(7s)$ threshold are presented in Fig. 4. Figure 5 shows the angular distribution asymmetry parameter β in the same energy region for all open channels except for those of $K(ns) + \epsilon p$ that have a constant value ($\beta=2$) due to symmetry considerations [30]. These two figures illustrate that each doubly excited state may produce very different resonance profiles in different partial cross sections as well as the β parameters. As shown in Fig. 6, the present results for $\sigma(5s)$ partial cross section, corresponding to the process $K^- + \gamma \rightarrow K(5s) + e^-$, agree in general with the relative measurements of Kiyani *et al.* [10], except for some discrepancies in the magnitude for photon energies above the $K(5d)$ and $K(7s)$ thresholds, and the slight shift in the position of the broad window near 4.22 eV. The letters a–c in Fig. 6 are the labels used in the experimental paper [10] for

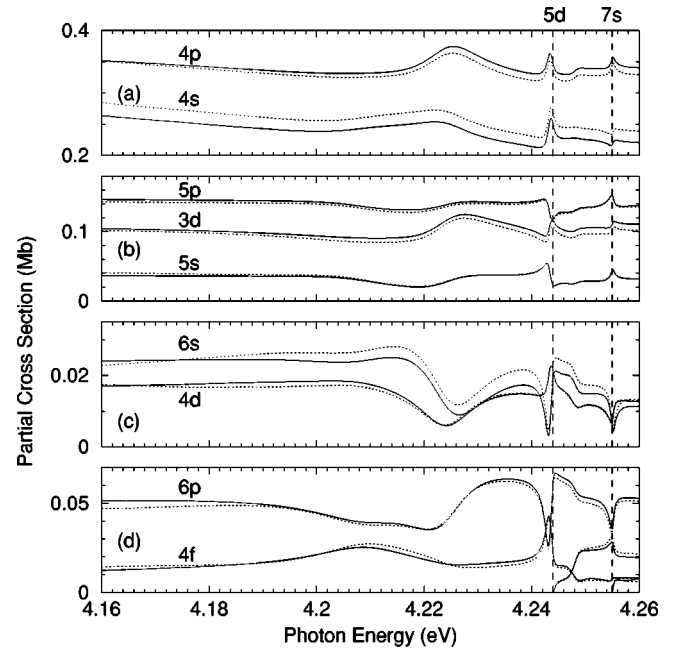


FIG. 4. Partial cross sections for the processes $K^- + \gamma \rightarrow K(nl) + e^-$, $nl=4s, 4p, 5s, 3d, 5p, 4d, 6s, 4f, 6p, 5d$, and $7s$. The solid (dotted) lines indicate present results in dipole velocity (length) approximation. The vertical dashed lines indicate the locations of the thresholds.

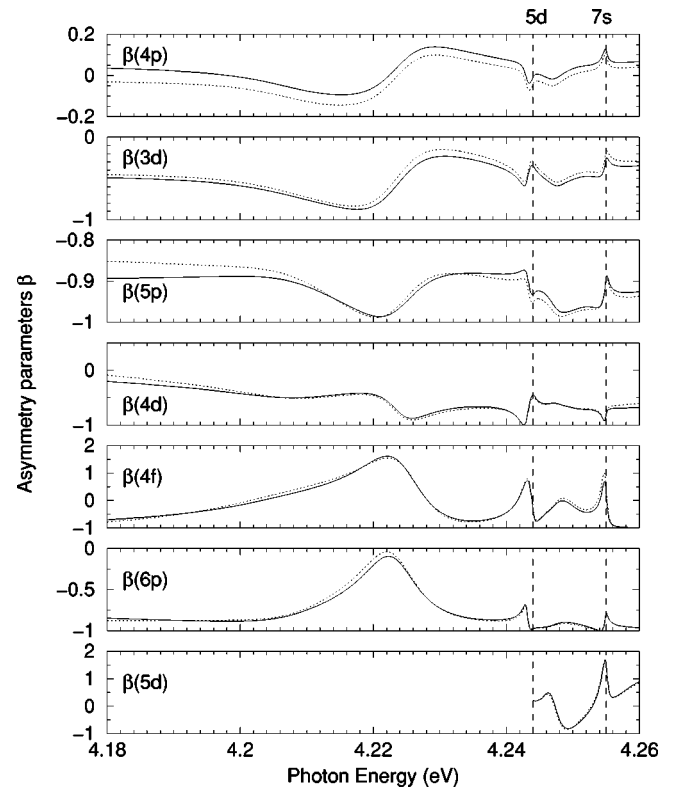


FIG. 5. Photoelectron angular distribution asymmetry parameters $\beta(nl)$. The solid (dotted) lines indicate present results in dipole velocity (length) approximation. The vertical dashed lines indicate the locations of the thresholds.

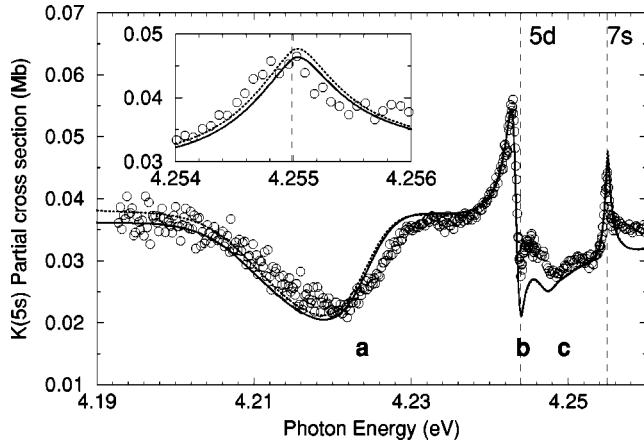


FIG. 6. Partial cross section for the process $K^- + \gamma \rightarrow K(5s) + e^-$ in the photon energy range from 4.19 to 4.26 eV. Curves: present results in dipole velocity (solid) and dipole length (dotted) approximations. Circles: relative experimental measurements of Kiyani *et al.* [10] normalized to the theoretical predictions. The inset shows a normalized comparison between theory and experiment near the $K(7s)$ threshold. The vertical dashed lines indicate the locations of the thresholds.

the resonances obtained by fitting the measured cross section to the Shore profile formula. In contrast to the experimental reporting of three resonances in this energy region, five resonances are identified in this work (cf. Table III), using the eigenphase sum analysis. The two additional resonances are located at 4.207 85 and 4.254 93 eV.

While there is only a visible window, labeled as resonance *a*, near 4.22 eV in the $\sigma(5s)$ partial cross section (cf. Fig. 6), the total cross section also suggests a single resonance [cf. Fig. 1(b)]. However, eigenphase sum analysis reveals that resonance *a* actually results from two overlapping resonances at 4.207 12 and 4.223 83 eV, respectively. The existence of two resonances is clearly indicated by other predictions in the present paper. For example, the $K(6p)$ partial cross section shows two overlapping windows whose locations are consistent with the predicted resonance energies [cf. Fig. 4(d) and Table III]. At the same positions, $\beta(4d)$ shows two dips (cf. Fig. 5). While the resonance at 4.223 83 eV dominates over the other at 4.207 12 in the total cross section, as well as in most of the partial cross section, the $K(4f)$ partial cross section exhibits a seemingly single, but weak, resonance peak at the position corresponding to the latter.

Applying the standard projection operator method with respect to the $K(5d)$ threshold one obtains three doubly excited states. The resonance at 4.207 12 eV is produced by a doubly excited state whose most important configurations are $5d7p$ (28.4%) and $6d5f$ (18.2%). In contrast, the one at 4.223 83 eV results from a perturber state associated with the higher $K(7s)$ threshold, indicated by its leading configurations $7s8p$ (17.3%), $7s7p$ (13.5%), and $5d6f$ (13.5%). Their configuration compositions are consistent with the weak interaction between the two states whose resonance profiles overlap. The leading configuration for the state responsible for the prominent resonance *b* at 4.243 30 eV are $5d9p$ (17.2%), $7s8p$ (16.0%), and $5d8p$ (14.1%). The pres-

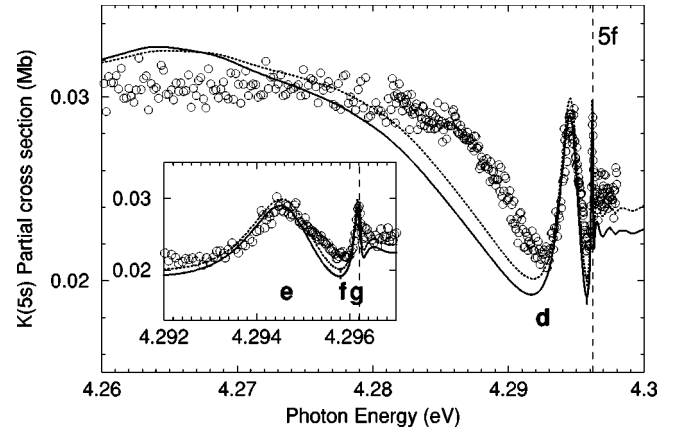


FIG. 7. Same as in Fig. 6 in the photon energy range from 4.26 to 4.30 eV. The inset shows the comparison between theory and experiment near the $K(5f)$ threshold.

ence of the configuration $7s8p$ indicates the influence of the perturber state.

To further identify the perturber state, projection operator methods are applied with respect to the $K(7s)$ state and two doubly excited states are found. Although all configurations involving the $5d$ orbital are removed, the one lower in energy actually coincides with the one responsible for the resonance at 4.223 83 eV located below the $K(5d)$ and $K(7s)$ thresholds overlap. This state plays a role as a perturber since it is associated with the higher-threshold $K(7s)$. The other is responsible for the resonance feature located just below the $K(7s)$ threshold at 4.254 98 eV, leaving the resonance located at 4.247 50 eV unexplained. However, based on these analyses, one may conclude that resonance *c* is not a resonance associated with $K(7s)$, but a core-excited resonance associated with $K(5d)$. This is consistent with the result from an eigenphase sum analysis, which shows an increase less than π in the vicinity of this resonance.

The inset of Fig. 6 clearly shows the calculated $\sigma(5s)$ partial cross section in the vicinity of the resonance located at 4.254 98 eV, just 0.01 meV below the $K(7s)$ threshold. Agreement with the measured $\sigma(5s)$ partial cross section is excellent in this small energy range. It is obviously incorrect to characterize this feature as a "threshold cusp" as in Ref. [10]. In this case, there is only one channel with a *p*-wave continuum associated with the $K(7s)$ excited state. Therefore, one would not expect a cusp behavior at the $K(7s)$ threshold. Indeed, the inset of Fig. 6 clearly shows that this is not a "threshold cusp." Actually, the $\sigma(5s)$ partial cross section is dominated by the resonance in the vicinity of the $K(7s)$ threshold, showing no visible threshold feature. An eigenphase sum analysis confirms the existence of a resonance.

D. K^- photodetachment below the $K(5f)$ threshold

Results for the $\sigma(5s)$ partial cross section in the energy region below the $K(5f)$ threshold are presented in Fig. 7 in a

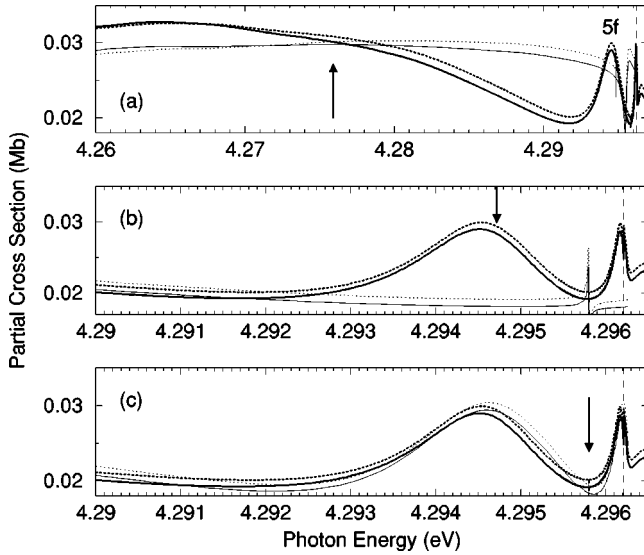


FIG. 8. Partial cross section for the process $K^- + \gamma \rightarrow K(5s) + e^-$ in the photon energy range from 4.26 to 4.30 eV. Thick curves: present results in dipole velocity (solid) and dipole length (dotted) approximations. Thin curves: results obtained by removing one or more doubly excited states from the calculations. The vertical dashed line indicates the location of the $K(5f)$ threshold. (a) The doubly excited state responsible for the resonance at 4.275 90 eV removed. (b) The doubly excited state responsible for the resonance at 4.294 72 eV removed. (c) The doubly excited state responsible for the resonance at 4.295 8031 eV removed. The arrows indicate the energy locations of the doubly excited state that has been removed from the cross-section result shown in the thin curve.

way similar to that of Sec. III C. The agreement between the calculated and measured results in this energy region is good, except for the discrepancy in the width of the window structure near 4.29 eV. Note that the calculated results in this region have been checked and confirmed. Also, the observed breadth of the resonance at 4.29 eV could be sensitive to the background variation in the relative measurements using a parallel beam arrangement. The present theoretical analysis reveals four resonances, which are as many as those presented in Ref. [10] by fitting the measured $\sigma(5s)$ partial cross section to the Shore formula. However, detailed characterization of these resonances revealed in the present analysis is quite different from the induced-dipole-potential model used in Ref. [10]. The standard projection operator method generates the wave functions of the doubly excited states responsible for these resonances, except for the one labeled as g due to its proximity to the $K(5f)$ threshold. Nevertheless, the eigenphase sum analysis confirms its location at 4.296 06 eV, just 0.15 meV below the $K(5f)$ threshold. Effects of these three doubly excited states are shown in Fig. 8, respectively.

While the results of fitting the measured $\sigma(5s)$ partial cross section assign the window centered at 4.292 eV as resonance d , Fig. 8(a) reveals that the corresponding doubly excited state produces an even broader feature. The leading configuration components for this broad resonance at 4.275 90 eV are $5f7d$ (21.6%), $6f5g$ (18.3%), and $5f6d$ (17.5%). Figure 8(b) shows a linear cross section and

an enhanced feature of the neighboring resonance f resulting from the second doubly excited state being removed, indicating that resonance e located at 4.294 72 eV manifests itself as a peak. This resonance is produced by a state whose major configuration components are $5f8d$ (19.2%), $8f5g$ (16.9%), and $5f9d$ (16.4%). Therefore, these two states responsible for resonances d and e share very similar $5fnd$ and $5gnf$ configuration compositions.

The measured $K(5s)$ partial cross section shows an extremely narrow resonance at 4.295 76 eV. The measured width of this resonance is 0.10 meV, which is far narrower than other features in the measured $K(5s)$ partial cross section. The current study predicts a resonance located at 4.295 803 1 eV with an even smaller width of 2 μ eV. Figure 8(c) shows that the narrow resonance removed after projecting out the corresponding doubly excited state. This resonance is produced by a state whose leading configurations are $7p6d$ (17.2%) and $8s7p$ (15.1%). In contrast to the states responsible for resonances d and e , there is almost no contribution from the $5fnd$ in its configuration composition. Also, there is no single strong $5fng$ component. Nevertheless, the collective contribution from the $5fng$ configurations for $5 \leq n \leq 9$ is about (17.6%). The diffused distribution of the $5fng$ configurations as well as the strong presence of $7pnl$ configurations might explain its very different character compared with the two lower resonances. Another more convincing evidence comes from the wave-function density plot of this state, which shows characteristics of a ground state in a series. Therefore, this state cannot possibly belong to the same series as the two lower resonances d and e . It is most likely a doubly excited state associated with the $K(7p)$ threshold, instead of the $K(5f)$ threshold.

E. K^- photodetachment below the $K(7p)$ threshold

The resonance structure in the total cross section in the energy region below the $K(7p)$ threshold is better illustrated in Fig. 9, showing a dominating broad resonance followed by a narrower one just below the $K(7p)$ threshold. The structure resembles the one in the energy region below the $K(6p)$ threshold [cf. Fig. (3)], except for the sloped background. In addition, the threshold behavior at the $K(7p)$ threshold also takes the form of a step. Another similarity is that there are no resonances associated with the next lower thresholds in each case [i.e., the $K(4f)$ and $K(5g)$ thresholds, which lie below the $K(6p)$ and $K(7p)$ thresholds respectively]. Both $K(4f)$ and $K(5g)$ have negative polarizabilities. Effects of each of the two resonances below the $K(7p)$ threshold are also shown in Fig. 9. While the state responsible for the broad resonance located at 4.323 39 eV is dominated by the configurations $7p8s$ (24.4%), $7p6d$ (24.0%), and $8p7d$ (16.6%), the other resonance located at 4.353 50 eV is produced by a state having strong configuration components $7p8d$ (28.1%) and $7p10s$ (20.0%).

IV. DISCUSSION

A complete list of energies and widths (when possible) for the present predictions for $^1P^o$ resonances in the energy re-

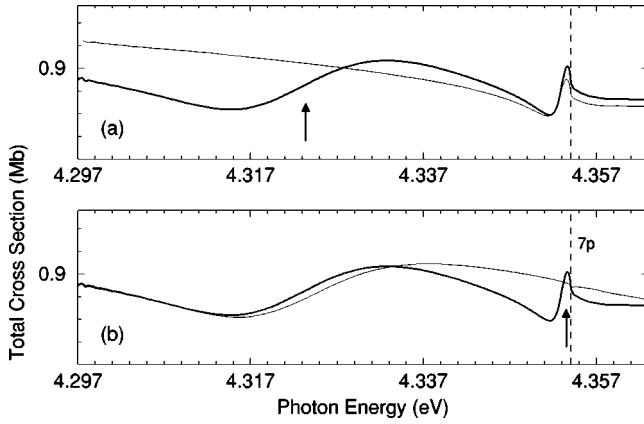


FIG. 9. Total cross section near the $K(7p)$ threshold. Thick curve: present results in dipole velocity approximation. Thin curve: results obtained by removing one doubly excited state from the calculation. The vertical dashed line indicates the location of the $K(7p)$ threshold. (a) The doubly excited state responsible for the resonance at 4.323 39 eV removed. (b) The doubly excited state responsible for the resonance at 4.353 50 eV removed. The arrows indicate the energy locations of the doubly excited state that has been removed from the cross-section result shown in the thin curve.

gion below the $K(7p)$ threshold is presented in Table II, together with recent experimental results from Kiyani *et al.* [10] obtained by fitting their measured partial cross section to the Shore profile formulas. Agreement between present predictions and the recent experimental measurements is good, except for resonances *a* and *d*. Although the experimental study assigned the window located at 4.292 eV in the $K(5s)$ partial cross section as resonance *a*, the present paper reveals that two overlapping resonances result in the observed window feature. One can see separate resonance profiles in, for example, the $\sigma(6p)$ partial cross section (cf. Fig. 4) or in $\beta(4d)$ (cf. Fig. 5). These examples suggest that fitting the measured cross section to a resonance profile formula might not be sufficient in determining resonance parameters. Also, the calculated the $K(5s)$ partial cross section deviates from the experimental results, as the theoretical prediction shows a much broader feature for the resonance *d*. Besides these resonances observed by Eyb [28] and Johnston and Burrow [27] (cf. Sec. IIIA), Zatsarinny *et al.* reveals a few autodetachment states in the same energy region by carrying out configuration-interaction calculations [31]. However, none of these resonances has a $^1P^o$ term value.

Combining current results and knowledge acquired from prior studies on He^- and alkali-metal negative ions [2–7,17,18], one may make more detailed comparisons between these systems with two active electrons and H^- , a pure three-body system. It has been shown that the adiabatical potential-energy curves of H^- in hyperspherical coordinates exhibit very close avoided crossings, reflecting weak channel interactions and the underlying approximate symmetry [32]. Also, propensity rules for radiative and nonradiative transitions are found, explaining characteristics of different resonance series [32,33]. Previous studies found that the resonance structures in the cross sections of He^- photodetachment reflect the same propensity rules [3]. In the cases of

negative alkali-metal ions, the energy levels of the neutral alkali-metal atom are not degenerate, resulting in complicated interchannel coupling and the breaking down of approximate symmetry. For example, there exists a very broad resonance in Li^- located between the $\text{Li}(3s)$ and $\text{Li}(3p)$ thresholds with a width of 0.36 eV [34]. In contrast, the width of the intrashell resonance in H^- in the $n=3$ manifold is only about 30 meV [34]. The breadth of the resonance in Li^- is due to the coupling between the closed $3p\epsilon s$ channel and the $3s\epsilon p$ continuum channel [34,35]. This kind of interchannel coupling does not occur in H^- . (Note that these channel notations are valid in the asymptotic region, where the independent-particle picture is adequate.) The predicted broad resonances in K^- at 4.030 92, 4.275 90, and 4.323 39 eV (cf. Fig. 1) are most likely due to a similar mechanism. Also, for alkali-metal atoms heavier than Li, the energy levels are no longer ordered according to their principal quantum numbers, indicating less hydrogenlike properties. Although the wave functions of the doubly excited states for the lighter negative alkali-metal ions, like Li^- and Na^- , still resemble the ones in H^- , the nodal structures become more obscure as the core becomes heavier [5,6]. However, the impact on the dynamics is more dramatic. For example, some doubly excited states are quasiforbidden in H^- photodetachment by propensity rules [32,33], but they produce resonance features that may be observed in photodetachment of alkali-metal negative ions [5]. One certainly observes the trend that, as the negative alkali-metal ions become heavier, the approximate symmetry of pure three-body systems is strongly modified by interchannel coupling.

Another profound difference resulting from the lack of degeneracy of the atomic levels is the asymptotic behavior of the electron-atom interaction, which plays a decisive role in the number of bound states. The interaction between an electron and an excited hydrogen atom has an asymptotic behavior like that of a permanent dipole potential, $V = -a/2r^2$, resulting in an infinite number of bound states if a is positive. Other than excited hydrogen, electron-atom interaction has the asymptotic form like that of an induced-dipole potential, $V = -\alpha/2r^4$, where α is the dipole polarizability of the corresponding atomic state. If $\alpha > 0$, such an asymptotically attractive potential may only support a finite number of bound states. Combining a long-ranged centrifugal potential, $l(l+1)/2r^2$, and an attractive induced-dipole potential results in a potential barrier in the asymptotic region. Such potential behavior could explain the common occurrence of shape resonances in negative ions. However, while a negative dipole polarizability implies an asymptotically repulsive potential, it does not necessary imply no bound state. A resonance associated with a state having a negative dipole polarizability was reported in Na^- [6]. Note that the induced-dipole behavior originating from the independent-particle picture is valid only in the asymptotic region, not in the region close to the nucleus, since the dominant electron-electron repulsion guarantees a repulsive effective potential in the vicinity of the nucleus. In fact, the electron correlation at a small distance from the nucleus plays an important role in the formation of bound states. Table IV shows the calculated dipole polarizabilities of the potassium states using the

model potential employed in the present study [cf. Eq. (1) and Table IV]. No predicted resonance in K^- in this paper is associated with a state of neutral potassium having a negative polarizability.

A semiclassical model based on a single-channel induced-dipole potential plus a centrifugal potential has been used to derive a formula describing resonance positions [2]. Results from recent experimental measurements are found to obey this formula [2,10]. Nevertheless, it is important to note that the attractive singularity of $1/r^4$ at $r=0$ due to the induced-dipole potential does not represent the correct repulsive potential behavior near the nucleus. Since the repulsive potential is very steep, the inner turning point is almost independent of energy. As a result, the phase of the WKB wave function has an almost constant contribution from the inner turning point, while the contribution from the outer turning point is sensitive to the energy and the asymptotic behavior of the potential. One may subsequently follow the same derivation applying the Bohr-Sommerfeld quantization rule as in Ref. [2] and obtain the same formula for resonance state spectrum. However, this formula may be applied only to a single series of resonances. The common occurrence of interchannel coupling in negative alkali-metal ions certainly limits the applicability of this formula. Also, without theoretical input, it is impossible to distinguish resonances when more than one series are involved. For example, the seven 4D resonances in He^- predicted in the vicinity of $He(n=5)$ thresholds belong to five different series characterized by their approximate quantum numbers [3].

The same semiclassical model has also been used to derive a formula describing resonance widths [11]. An anomalous behavior is predicted that, as a series of resonances approaches the corresponding threshold, the widths do not necessarily decrease monotonically. Resonance f was considered as evidence for the anomalous width behavior [11]. But, this formula for resonance widths resulting from an inaccurate assumption on the potential in the region near the nucleus is questionable. Since the wave function of the doubly excited state responsible for resonance f shows charac-

teristics of the lowest state of the corresponding series, resonance f cannot possibly belong to the same series as the two lower resonances d and e . Therefore, it is incorrect to assume that all four observed resonances below the $K(5f)$ threshold belong to a single series.

V. CONCLUSIONS

A detailed study for K^- photodetachment over the energy region from the $K(5s)$ threshold to the $K(7p)$ threshold has been presented. The present results for the $K(5s)$ partial cross section between the $K(6p)$ and $K(5f)$ thresholds are in good agreement with the recent measurements of Kiyan *et al.* [10]. Using the standard projection operator method, all $^1P^o$ resonances in the energy region studied are analyzed and their corresponding doubly excited states are identified. A complete list of energies and widths for these predicted $^1P^o$ resonances is given. An example is found that two overlapping resonances results in a single window feature observed in the $K(5s)$ cross section, thus suggesting that fitting the measured cross section to a resonance profile formula might not be sufficient in determining resonance parameters. Comparing current results and prior studies on He^- and other alkali-metal negative ions, one observes that, as the alkali-metal negative ions become heavier, the approximate symmetry of pure three-body systems breaks down, replaced by complicated interchannel coupling. The asymptotic behavior of electron-atom interaction plays a decisive role in the structure of negative ions. However, a pure induced-dipole potential is not sufficient to describe the structure and dynamics of nonhydrogenic negative ions. One has to take into account effects due to interchannel coupling and electron correlation in the region close to the nucleus.

ACKNOWLEDGMENTS

The author thanks A.F. Starace and C.D. Lin for valuable discussions. He also thanks I. Yu. Kiyan for providing the experimental data of Ref. [10].

-
- [1] See, for example, P. Balling, H.H. Andersen, C.A. Brodie, U.V. Pedersen, V.V. Petrunin, M.K. Raarup, P. Steiner, and T. Andersen, *Phys. Rev. A* **61**, 022702 (2000), and references therein.
- [2] I.Yu. Kiyan, U. Berzinsh, D. Hanstorp, and D.J. Pegg, *Phys. Rev. Lett.* **81**, 2874 (1998).
- [3] C.N. Liu and A.F. Starace, *Phys. Rev. A* **60**, 4647 (1999).
- [4] U. Ljungblad, D. Hanstorp, U. Berzinsh, and D.J. Pegg, *Phys. Rev. Lett.* **77**, 3751 (1996).
- [5] C.N. Liu and A.F. Starace, *Phys. Rev. A* **58**, 4997 (1998).
- [6] C.N. Liu and A.F. Starace, *Phys. Rev. A* **59**, 3643 (1999).
- [7] G. Haeffler, I.Yu. Kiyan, D. Hanstorp, B.J. Davies, and D.J. Pegg, *Phys. Rev. A* **59**, 3655 (1999).
- [8] See, for example, K.T. Taylor and D.W. Norcross, *Phys. Rev. A* **34**, 3878 (1986), and references therein.
- [9] See the review by S.J. Buckman and C.W. Clark, *Rev. Mod. Phys.* **66**, 539 (1994), and references therein.
- [10] I.Yu. Kiyan, U. Berzinsh, J. Sandström, D. Hanstorp, and D.J. Pegg, *Phys. Rev. Lett.* **84**, 5979 (2000).
- [11] I.Yu. Kiyan, *Phys. Rev. Lett.* **84**, 5975 (2000).
- [12] D.R. Herrick, *Phys. Rev. A* **12**, 413 (1975); *Adv. Chem. Phys.* **52**, 1 (1983).
- [13] C.D. Lin, *Phys. Rev. A* **29**, 1019 (1984); *Adv. At. Mol. Phys.* **22**, 77 (1986).
- [14] J.M. Feagin and J.S. Briggs, *Phys. Rev. Lett.* **57**, 984 (1986); *Phys. Rev. A* **37**, 4599 (1988).
- [15] U. Fano and C.M. Lee, *Phys. Rev. Lett.* **31**, 1573 (1973).
- [16] P.F. O'Mahony and C.H. Greene, *Phys. Rev. A* **31**, 250 (1985); C.H. Greene and L. Kim, *ibid.* **36**, 2706 (1987); C.H. Greene and L. Kim, *ibid.* **38**, 5953 (1988); C. H. Greene, in *Fundamental Processes of Atomic Dynamics*, edited by J. S. Briggs, H. Kleinpoppen, and H. O. Lutz (Plenum, New York, 1988), pp. 105–127.

- [17] C. Pan, A.F. Starace, and C.H. Greene, *J. Phys. B* **27**, L137 (1994).
- [18] C. Pan, A.F. Starace, and C.H. Greene, *Phys. Rev. A* **53**, 840 (1996).
- [19] W.R. Johnson, D. Kolb, and K.-N. Huang, *At. Data Nucl. Data Tables* **28**, 333 (1982).
- [20] C. E. Moore, *Atomic Energy Levels*, Natl. Bur. Stand. (U.S.) Circ. No. NSRDS-NBS35 (U.S. GPO, Washington, D.C., 1971).
- [21] U. Fano, *Phys. Rev.* **124**, 1866 (1961).
- [22] B.W. Shore, *Phys. Rev.* **171**, 43 (1968).
- [23] A.F. Starace, *Phys. Rev. A* **16**, 231 (1977).
- [24] R.K. Nesbet and J.D. Lyons, *Phys. Rev. A* **4**, 1812 (1971).
- [25] A.U. Hazi, *Phys. Rev. A* **19**, 920 (1979).
- [26] K.T. Andersson, J. Sandström, I.Yu. Kiyani, D. Hanstorp, and D.J. Pegg, *Phys. Rev. A* **62**, 022503 (2000).
- [27] A.R. Johnston and P.D. Burrow, *Phys. Rev. A* **51**, 406 (1995).
- [28] M. Eyb, *J. Phys. B* **9**, 101 (1976).
- [29] E.P. Wigner, *Phys. Rev.* **73**, 1002 (1948).
- [30] S.T. Manson and A.F. Starace, *Rev. Mod. Phys.* **54**, 389 (1982).
- [31] O.I. Zatsarinny, V.I. Lengyel, E.P. Sabad, and I.I. Cherlenyak, *Izv. Akad. Nauk SSSR, Ser. Fiz.* **50**, 1377 (1986).
- [32] H.R. Sadeghpour and C.H. Greene, *Phys. Rev. Lett.* **65**, 313 (1990); H.R. Sadeghpour, *Phys. Rev. A* **43**, 5921 (1991).
- [33] J.M. Rost and J.S. Briggs, *J. Phys. B* **23**, L339 (1990); A. Vollweitwer, J.M. Rost, and J.S. Briggs, *ibid.* **24**, L115 (1991).
- [34] E. Lindroth, *Phys. Rev. A* **52**, 2737 (1995).
- [35] C.D. Lin, *J. Phys. B* **16**, 723 (1983).